CrossMark

Chitosan-based composite bilayer scaffold as an *in vitro* osteochondral defect regeneration model

Ariane E. Erickson[1] · Jialu Sun[1] · Sheeny K. Lan Levengood[1] · Shawn Swanson[1] · Fei-Chien Chang[1] · Ching T. Tsao[1] · Miqin Zhang[1]

Abstract

Prolonged osteochondral tissue damage can result in osteoarthritis and decreased quality of life. Multiphasic scaffolds, where different layers model different microenvironments, are a promising treatment approach, yet stable joining between layers during fabrication remains challenging. Here, a bilayer scaffold for osteochondral tissue regeneration was fabricated using thermally-induced phase separation (TIPS). Two distinct polymer solutions were layered before TIPS, and the resulting porous, bilayer scaffold was characterized by seamless interfacial integration and a mechanical stiffness gradient reflecting the native osteochondral microenvironment. Chitosan is a critical component of both scaffold layers to facilitate cell attachment and the formation of polyelectrolyte complexes with other biologically relevant natural polymers. The articular cartilage region was optimized for hyaluronic acid content and stiffness, while the subchondral bone region was defined by higher stiffness and osteoconductive hydroxyapatite content. Following co-culture with chondrocyte-like (SW-1353 or mesenchymal stem cells) and osteoblast-like cells (MG63), cell proliferation and migration to the interface along with increased gene expression associated with relevant markers of osteogenesis and chondrogenesis indicates the potential of this bilayer scaffold for osteochondral tissue regeneration.

Keywords Chitosan · Hyaluronic acid · Alginate · Hydroxyapatite · Osteochondral defect · Bilayer scaffold

1 Introduction

Osteochondral tissue is composed of an articular cartilage region and a subchondral bone region with a calcified cartilage interface linking the two distinct microenvironments. Osteochondral defects arise when damage or disease affect both regions (Hunziker 2002) and surgical treatment options vary from bone marrow stimulation to chondrocyte and/or graft transplantation (Bekkers et al. 2012; Cole et al. 2009). However, these treatments are associated with inherent complications (Bexkens et al. 2017; Hunziker 2002; Lopez-Ruiz et al. 2016; Smith et al. 2005). For example, therapies only targeting the cartilage zone without consideration of the

interface or subchondral bone result in increased defect size, a weak tissue interface, and structural degradation of the underlying bone (Madry et al. 2010; Schinhan et al. 2012). Regeneration of osteochondral defects is nontrivial and requires synchronized vascularization and calcification in the bone region concurrently with avascular collagen deposition in the cartilage region (Hunziker 2002).

Tissue engineering (TE) scaffolds provide a three-dimensional (3D), biodegradable template for cell attachment/differentiation. TE scaffolds can be utilized for treatment of osteochondral defects by providing synchronized, yet segregated support of two or more distinct cell populations with differing biochemical and biomechanical requirements. In monophasic scaffolds, extent of osteochondral tissue regeneration is low relative to multiphasic scaffolds indicating that monophasic materials may be inadequate mimics of the native microenvironment and therefore unable to simultaneously support chondrogenesis and osteogenesis (Seo et al. 2014; Singh et al. 2018). Thus, various bilayer and multilayer (3+ layers) 3D, porous scaffolds have been fabricated to address the unique characteristics of the osteochondral microenvironment. Porous scaffolds that mimic osteochondral extracellular matrix (ECM)

✉ Miqin Zhang
mzhang@u.washington.edu

[1] Department of Materials Science & Engineering, University of Washington, Seattle, WA 98195, USA

are fabricated with a wide range of physical properties including tailored pore size (Di Luca et al. 2016; Nie et al. 2016; Oh et al. 2007), pore shape, (Aydin 2011) mineral content (Kon et al. 2010; Yusong et al. 2013), or biochemical gradients (Levingstone et al. 2014; Oh et al. 2011). These studies demonstrate the efficacy of multilayer or multiphasic scaffolds *in vitro* (Galperin et al. 2013; Levingstone et al. 2014) and *in vivo* (He et al. 2017; Levingstone et al. 2016). Although promising, limitations of multiphasic scaffolds include time-consuming, iterative fabrication or joining procedures, as well as inadequate or unstable interfacial regions between layers (Hunziker and Driesang 2003; Levingstone et al. 2014). These significant limitations indicate a need for further innovation in the design and optimization of such scaffolds for osteochondral tissue engineering.

Synthetic polymers are often utilized in bone tissue engineering due to their superior mechanical integrity relative to natural polymers. However, synthetic polymers have slow degradation rates, harmful degradation products, and lack cell attachment and differentiation cues (Schaefer et al. 2002). Natural polymers are more biocompatible, but their mechanical properties are suboptimal for many tissue engineering applications. Polyelectrolyte complexes (PECs), such as chitosan-alginate (Florczyk et al. 2011; Li and Zhang 2005) and chitosan-hyaluronic acid, (Florczyk et al. 2013), formed via ionic interactions between natural cationic and anionic polymers, possess enhanced integrity and stiffness. Further, the integration of bioactive cues such as hyaluronic acid (HA), a glycosaminoglycan (GAG) found in articular cartilage, improves chondrocyte attachment and chondrogenic differentiation (Galperin et al. 2013; Kim et al. 2003; Yoo et al. 2005). Bone scaffolds frequently contain osteoconductive materials, such as tricalcium phosphate or hydroxyapatite (HAp), to stimulate osteoblastic activity, increase scaffold stiffness, and induce influence phenotypic expression in osteoblast-like cells (Galperin et al. 2013). The incorporation of bioactive cues specific to the distinct microenvironments present in native osteochondral tissue can promote tissue regeneration (Galperin et al. 2013; Kim et al. 2003; Shu et al. 2003; Yoo et al. 2005).

In this study, we present a bilayer scaffold with a stable, calcified transition zone fabricated via a thermally-induced phase separation (TIPS) fabrication process. The scaffold has two regions. The first region, a chitosan-hyaluronic acid cartilage layer, is defined by relatively lower stiffness and the presence of hyaluronic acid (HA). The second region, a chitosan-alginate bone layer, was optimized for higher stiffness and osteoconductive hydroxyapatite nanorod (6% CA + HAp) content. Chitosan was selected as a major component of the bilayer scaffold as it supports attachment and proliferation of both osteoblasts (Levengood and Zhang 2014; Li et al. 2005) and chondrocytes (Li and Zhang 2005). This report describes how each layer of the scaffold, or each base scaffold, was optimized to reflect structural, physical, and biological properties unique to the osteochondral microenvironment. The scaffold design process required a multi-step optimization involving material characterization and *in vitro* cell-based evaluation. By combining two distinct scaffolds optimized for cartilage and bone, respectively, using TIPS fabrication processes, a region between the two layers was established, resulting in a gradient transition zone with increasing stiffness and calcium content resembling that of native osteochondral tissue. The biological performance of the optimized scaffold was characterized to investigate scaffold potential for osteochondral tissue engineering applications.

2 Experimental

2.1 Materials

Unless otherwise stated, all chemicals were purchased from Sigma Aldrich and used as received. Scaffolds were synthesized using chitosan (from shrimp shells, practical grade, MW = 190–375 kDa, $\geq$ 75% deacetylated), hyaluronic acid sodium salt (from *Streptococcus equi*, MW = 1.5–1.8 × 10^6 Da) and alginic acid sodium salt (from brown algae, medium viscosity). All tissue culture reagents (antibiotic-antimycotic (AA), Dulbecco's phosphate buffered saline (D-PBS), Dulbecco's modified Eagle medium (DMEM), TripLE, trypsin, and fetal bovine serum (FBS)) were purchased from Life Technologies. Human chondrocyte-like (SW-1353) and human osteoblast-like (MG63) cells were used as received (American Type Culture Collection, Manassas, VA). Rat bone marrow derived mesenchymal stem cells (MSC) were isolated from Sprague-Dawley rat bone marrow aspirate as previously described (Florczyk et al. 2012) and cultured in fully supplemented DMEM. Cells were maintained according to manufacturer's instructions in fully supplemented DMEM with 10% FBS and 1% AA at 37 °C and 5% CO_2 in a fully humidified incubator.

2.2 Scaffold fabrication

2.2.1 Base scaffold

Six different scaffolds (Table 1) were fabricated for optimization of the base scaffolds for the cartilage or bone regions. Pure chitosan (C) (Jana et al. 2012), chitosan-alginate (CA) (Florczyk et al. 2016; Kievit et al. 2010), and chitosan-hyaluronic acid (CHA) (Florczyk et al. 2013; Wang et al. 2016) were prepared as previously reported. During scaffold fabrication, all homogenization steps were performed three times at 2000 RPM for 3 min using a Thinky mixer (ARM-300, Thinky USA, Laguna Hills, CA).

4 wt% pure chitosan scaffolds (4% C) were fabricated by first adding 4 g of chitosan to a 1 wt% acetic acid solution. For 6 wt% pure chitosan scaffolds (6% C), 6 g of chitosan were added to a 2 wt% acetic acid solution. The higher acetic acid

Table 1 Scaffold naming nomenclature and composition

Scaffold Type	Solution Fabrication (wt%)		Total Polymer (wt%)
	Step 1	Step 2	
4% C	4% C in 1% AA	–	4% C
6% C	6% C in 2% AA	–	6% C
4% CA	2% A in DI water	2% C in 0.5% AA	2% A + 2% C = 4% CA
6% CA	3% A in DI water	3% C in 1% AA	3% A + 3% C = 6% CA
4% CHA	4% C in 1% AA	1% HA in 1% AA	2% C + 0.5% HA = 2.5% CHA
6% CHA	6% C in 2% AA	1% HA in 1% AA	3% C + 0.5% HA = 3.5% CHA

C, chitosan; A, alginate; HA, hyaluronic acid; AA, acetic acid; CA, chitosan+alginate; CHA, chitosan+hyaluronic acid

concentration was used to ensure dissolution of chitosan at the higher polymer concentration. Both solutions were homogenized, aged overnight at room temperature to ensure complete dissolution, and cast into a 24-well plate at 3 mL per well.

To fabricate 4 wt% chitosan-alginate scaffolds (4% CA), 4 g of alginate were dissolved in 199 mL of DI water and stirred using a Thinky mixer. Upon alginate dissolution, chitosan (4 g) and acetic acid (1 g) were added and the solution was homogenized until dissolved. For 6% CA scaffolds, 6 g of alginate was dissolved in 198 mL of DI water followed by the addition of 6 g of chitosan and 2 g of acetic acid. Upon chitosan dissolution, the polymer solutions were mixed in a blender for 5 min, cooled in a cold-water bath to prevent polymer solution overheating, and mixed in a blender again for 5 min. The scaffold solution was cast into a 24 well-plate at 3 mL per well.

4 wt% chitosan – hyaluronic acid (4% CHA) scaffolds were fabricated by first preparing the chitosan and HA polymer solutions separately. Chitosan (4 wt%) and HA (1 wt%) were separately dissolved in 1 wt% acetic acid. For 6% CHA scaffolds, chitosan (6 wt%) was dissolved in 2 wt% acetic acid, to ensure dissolution of chitosan at the higher polymer concentration. The HA solution was created by dissolving 1 wt% HA in a 1 wt% acetic acid solution. Chitosan and HA polymer solutions were individually homogenized and aged overnight at room temperature. After dissolution, chitosan and HA polymer solutions were combined, homogenized, and mixed in a blender for one min. The resultant polymer solution was cast into a 24-well plate at 3 mL per well.

All 24-well plates containing the polymer solutions were centrifuged for 1–5 min at 2000 RPM to remove air bubbles, refrigerated for >12 h, frozen at −20 °C for >24 h, and lyophilized using a Labconco Freezone 6 freeze dryer.

Table 1 summarizes the scaffold naming conventions. Naming conventions are based on a ratio of polymer mass to total solution volume. Specifically, for pure chitosan (C) scaffolds, the total polymer content (wt%) was equivalent to the amount of solubilized chitosan. A 6% pure chitosan scaffold contains 6 wt% chitosan. For CA scaffolds, the total polymer content was equivalent to the amount of solubilized chitosan plus the amount of solubilized alginate. A 6% CA scaffold contained 3 wt% chitosan and 3 wt% alginate for a 6 wt% total polymer content.

HA has poor solubility and high viscosity at moderate concentrations. Therefore, 1 wt% HA was the highest concentration used. The association between the naming convention of CHA scaffolds and the total polymer content is different from the C and CA scaffolds. Importantly, the naming convention, which is based on the chitosan concentration prior to blending, remains consistent with scaffolds presented in literature (Florczyk et al. 2013). A 6% CHA scaffold contains a 6 wt% chitosan solution blended with a 1 wt% HA solution for a total of 3.5 wt% polymer.

2.2.2 Composite chitosan-alginate + hydroxyapatite scaffolds

Hydroxyapatite nanorods (HAp) were synthesized based on a previously reported procedure (Jin et al. 2015) with slight modifications to obtain processing conditions encompassing ambient pressure and body temperature. Briefly, 0.75 M sodium citrate was added dropwise to 0.1 M calcium nitrate. Sodium hydroxide was used to adjust pH to 9 and the solution was aged for 30 min at room temperature. A 0.06 M sodium phosphate monobasic solution was prepared, adjusted to pH 9, and then aged for 30 min. Under constant stirring, the solutions were mixed to achieve a precipitate with a Ca/P ratio of 1.67. The mixture was heated to 37 °C under constant stirring for 2 days while maintaining a pH of 9. The nanorod precipitate (HAp) was filtered, washed with DI water, and dried at 70 °C overnight. The length of the nanorods was 80.0 ± 25.4 nm and width was 6.7 ± 4.0 nm ($n = 20$ nanorods). Nanorod morphology was observed with transmission electron microscopy (TEM). HAp was added to a 6% CA polymer solution (synthesis outlined above) to obtain concentrations of 0.1 wt%, 0.25 wt%, 0.5 wt%, 1 wt%, 2 wt%, and 3 wt% HAp. The composite polymer solution was blended, homogenized, and cast in a 24-well plate at 3 mL per well. The plate was centrifuged at 1000 RPM for 5 min, refrigerated for >12 h, placed in a −20 °C freezer for >24 h, and lyophilized using a Labconco freeze dryer.

2.2.3 Bilayer scaffolds

The complete bilayer scaffold fabrication process is summarized in Fig. 1a. During scaffold fabrication, all homogenization steps were conducted using a Thinky mixer three times at 2000 RPM for 3 min. Solutions for each layer of the bilayer scaffold were prepared separately. For the cartilage layer, a 4% CHA solution was produced by dissolving chitosan (4 wt%) and HA (1 wt%) separately in 1 wt% acetic acid. Chitosan and HA solutions were individually homogenized and aged overnight at room temperature. The polymer solutions were then homogenized and mixed in a blender for 1 min. Wells of a 24-

(a)

Cartilage Layer
4% chitosan + 1% hyaluronic acid

Bone Layer
6% chitosan + 6% alginate + 0.5% hydroxyapatite

4% C   1% HA

4% CHA

Homogenize

Peristaltic pump

Age 48 hours at 37°C

$Ca(NO_3)_2$ Na_2HPO_4

HAp Synthesis

0.5% HAp   6% C   6% A

6% CA+0.5% HAp

Homogenize

Layer, centrifuge, freeze, and lyophilize to fabricate bilayer scaffolds.

4% CHA

Firm gel 1 hr at 4°C

6% CA + 0.5% HAp

4% CHA

Centrifuge, freeze at 20°C, and lyophilize

Cartilage Layer 4% CHA

Bone Layer 6% CA + 0.5% HAp

(b)

Co-culture cell seeding in bilayer scaffold.

SW-1353 or MSC

Attach for 2 hours, flip, and seed other side

MG63

Attach for 2 hours and add media

SW-1353 or MSC
+
MG63

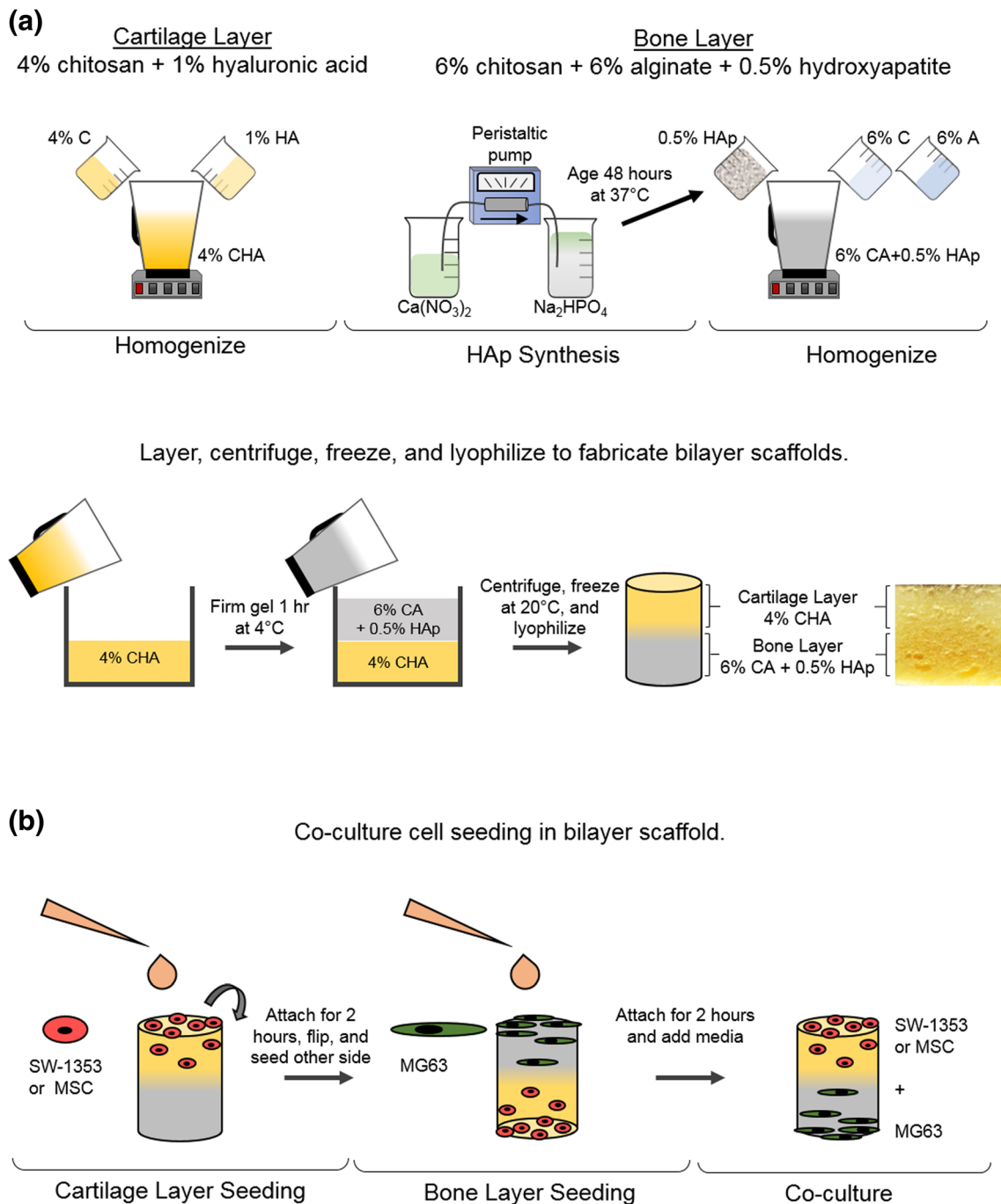Cartilage Layer Seeding

Bone Layer Seeding

Co-culture

Fig. 1 Bilayer scaffold synthesis and co-culture cell seeding. **a** The three-step fabrication process includes: (1) synthesis of HAp nanorods using a chemical precipitation method, (2) individual preparation of the 4% CHA and 6% CA + HAp solutions, and (3) layering the two polymer solutions, centrifuging, freezing, and lyophilizing to achieve a gradient scaffold with an integrated interface region. **b** Co-culture seeding scheme in the bilayer scaffold where SW-1353 or MSC cells are first seeded in the cartilage layer (4% CHA), the scaffold is then flipped, and MG63 cells are seeded in the bone layer (6% CA + HAp)

well plate were filled with 1.5 mL of the 4% CHA polymer solution per well. The plate was then centrifuged and refrigerated for 1 h to yield a firmer and more viscous solution. For the bone layer, a 6% CA + 0.5% HAp material solution was prepared by dissolving 6 g of alginate in 198 mL of DI water and homogenizing. Upon dissolution, chitosan (6 g) and acetic acid (2 g) were added and the solution was homogenized, mixed in a blender for 5 min, and cooled in a cold-water bath. Hydroxyapatite nanorods (0.5 wt%) were then dispersed in the CA polymer solution. The 6% CA + HAp polymer solution was blended for 5 min and then mixed at 2000 RPM for 3 min with a Thinky mixer to eliminate bubbles. 1.5 mL of the CA polymer solution was gently cast in each well on top of the refrigerated 4% CHA solution in a 24-well plate. The layered polymer solutions were then centrifuged at 2000 RPM for 5 min. This centrifugation step eliminated air bubbles at the interface thereby integrating the two layers and preventing delamination. The scaffolds were then refrigerated for >12 h, frozen at −20 °C for >24 h and lyophilized using a Labconco freeze dryer.

2.2.4 Scaffold neutralization and sterilization

All base and HAp-integrated single-phase scaffolds had a diameter of ~15 mm and a thickness of 10 mm and were cut into 3 mm-thick disks, and neutralized and/or crosslinked as summarized in Table S1. The cylindrical bilayer scaffolds were 6 mm tall with an approximate diameter of 15 mm. Scaffolds were cut into four quarters, and simultaneously neutralized and crosslinked. Neutralization, crosslinking, and sterilization steps were conducted under vacuum. All crosslinked/ neutralized scaffolds were rinsed 3 times with DI water, and soaked in D-PBS or DI water on a shaker at 60 RPM overnight. After ethanol sterilization, all scaffolds were rinsed three times and soaked overnight in sterile D-PBS to remove residual ethanol. Before cell seeding, the scaffolds were transferred to fully supplemented cell culture media for at least 2 h.

2.3 Microscopy

Scaffold pore morphology was visualized with a scanning electron microscope (SEM, JEOL JSM-7000F). Specifically, dry scaffolds were mounted on stubs using carbon tape and coated with Au/Pd for 60 s before imaging. HAp nanorod samples were prepared using a copper grid and imaged with a Transmission Electron Microscope (TEM, Philips EM430 TEM).

2.4 Pore size measurement

Individual pore areas were measured from SEM micrographs using ImageJ software. At least 14 pores were measured per base scaffold condition to determine mean pore area. For the bilayer scaffold, > 35 pores were measured in each layer. Pores were outlined using the freehand selection function in ImageJ and the area measured. Pore diameter was estimated using the mean pore area and assuming pores were a perfect circle.

2.5 Mechanical testing

Compression testing was conducted with a Shimadzu Universal tester (AGS-X) using a 100 N load cell at a strain rate of 0.4 mm/min. Scaffolds were cut into 2-mm thick disks and tested in dry and hydrated states. Hydrated samples were crosslinked and/or neutralized and soaked in D-PBS for >1 h prior to testing. Testing of bilayer scaffolds was conducted using full thickness (6-mm height) hydrated scaffolds. At least four samples were tested per condition.

2.6 Porosity and density measurements

Bulk density of each scaffold was determined by measuring the scaffold mass to the ten-thousandth of a gram and the scaffold diameter using micrometers ($n = 12$). Porosity of bilayer scaffolds was measured using a modified liquid displacement method.(Hsu et al. 1997; Zhang and Ma 1999) Specifically, the weight (W_i) and volume (V_i) of a dry scaffold was recorded. The scaffold was fully submerged in isopropanol for 20 min under vacuum. The isopropanol-impregnated scaffold was weighed (W_f). Scaffold porosity ($n = 5$) was calculated as a ratio of the volume of the solvent in the scaffold pores to the volume of the dry scaffold as shown in Eq. 1, where ρ is the density of isopropanol. Weight was measured in mg, and volume was measured in mm^3.

$$\text{Porosity} = \frac{(W_f - W_i)/\rho}{V_i} \times 100 \qquad (1)$$

2.7 Cell seeding and cell proliferation in base scaffolds

Base scaffolds were seeded with 20,000 SW-1353, MSC, or MG63 cells suspended in 50 μL of fully supplemented DMEM. Scaffolds were incubated for 2 h to allow for cell infiltration and attachment before adding fully supplemented media. Media were changed every 2–3 days for the 14-day culture period. Cell proliferation was evaluated at 2, 7, and 10 days using 10% alamarBlue® reagent in fully supplemented media ($n = 4$ per condition). Scaffolds were incubated for 4 h in the alamarBlue® solution before an aliquot of the solution was transferred to an opaque black 96-well plate. Fluorescence intensity was measured using a SpectraMax M5 microplate reader (Molecular Devices, Union City, CA)

at an excitation wavelength of 560 nm and emission wavelength of 590 nm. Fluorescence intensity was converted to cell number based on standard curves created for each scaffold type/cell line. Excess alamarBlue® was aspirated and scaffolds were washed with D-PBS before fresh media was added after each timepoint.

2.8 Cell seeding, cell proliferation, and live cell imaging in bilayer scaffolds

One cell type was seeded into each layer of the bilayer scaffolds to evaluate metabolic activity of co-cultures (SW-1353 + MG63 or MSC + MG63) (Fig. 1b). This culture condition is referenced throughout the text as a "co-culture." In the cartilage region, 200,000 cells (SW-1353 or MSC) suspended in 100 μL of fully supplemented DMEM were seeded into the 4% CHA layer and incubated for 2 h to allow cell infiltration and attachment. Scaffolds were then flipped and 200,000 MG63 cells in 100 μL of fully supplemented DMEM were seeded in the 6% CA + HAp layer. The scaffold was again incubated for 2 h before the addition of fully supplemented media. Media were changed every 2–3 days over the 14-day culture period.

Proliferative capacity (n = 4) was determined at 2, 4, 7, 10, and 14 days using the alamarBlue® assay. Scaffolds containing cells and blank scaffolds were incubated for 4 h in alamarBlue® solution. Then an aliquot of the solution was transferred to an opaque black 96-well plate. Fluorescence intensity was measured using a SpectraMax M5 microplate reader (Molecular Devices, Union City, CA) at an excitation wavelength of 560 nm and emission wavelength of 590 nm. The measured fluorescence intensity from scaffolds cultured with cells was normalized to the measured fluorescence intensity associated with blank scaffolds. The fluorescence intensity correlates with the metabolic activity of each culture condition. Excess alamarBlue® was aspirated and scaffolds were washed with D-PBS before fresh media was added after each timepoint.

To view cell distribution and infiltration into the bilayer scaffold, live cell images were acquired using a Nikon inverted fluorescent microscope with appropriate filters on a Nikon Ri1 Color Cooled Camera system (Nikon instruments, Melville, NY). To differentiate cells seeded in each layer of the bilayer scaffolds, the SW-1353 or MSC cells were stained with red Vybrant® DiI cell-labeling (Molecular Probes, Thermo Fisher) rendering the cells red-orange when excited at 549 nm (565 nm emission). Cells (SW-1353 or MSC) were incubated for 30 min in red Vybrant® DiI at 1 μg/mL in D-PBS prior to seeding in the cartilage layer. MG63 cells were seeded in the bone layer with no prior staining. Before imaging after 1 and 14 days of culture, the entire bilayer scaffold was incubated for 30 min in 5 μM calcein AM (Thermo Fisher) in D-PBS. Calcein AM is a cell-permeant dye that is converted from colorless to a green-fluorescent calcein after

hydrolysis when excited at 495 nm (emission 515 nm), and therefore can be used for determination of live cells. Cells in the cartilage layer, SW-1353 or MSC, were double stained and emitted both red and green fluorescence, depending on the excitation wavelength, and in the bone layer, MG63 were identified as green with no red signal. After merging images using ImageJ and Adobe Photoshop, differences in excitation wavelength between DiI (red) and calcein AM (green) stained cells allowed cells in the cartilage layer (SW-1353 or MSC) to be visualized as red-orange and bone layer cells (MG63) to be visualized as green.

2.9 PCR

After two weeks of culture, cells were detached from the bilayer scaffolds using TripLE Express and ribonucleic acid (RNA) was extracted following the manufacturer's protocol using the Qiagen RNeasy kit (Qiagen, Valencia, CA). Following the manufacturer's instructions, iScript cDNA synthesis kit (Bio-Rad, Hercules, CA) was used for reverse transcription (RT) to prepare cDNA. DNA transcripts were probed using SoAdvanced Universal SYBR Green Supermix (Bio-Rad) with the primers listed in Table S2. Thermocycling was performed on 10 μL of solution containing 5 μL SYBR Supermix, 300 nM primers (Integrated DNA Technologies, Coralville, IA), and cDNA concentrated at 4 ng/μL. The thermocycling was performed using the BioRad CFX96 System at 95 °C for 3 min, 40 cycles at 95 °C for 15 s, and 60 °C for 1 min. All qRT-PCR data was analyzed with the CFX Manager software (Bio-Rad) where expression levels were normalized to a reference gene, GAPDH. Gene expression between conditions was normalized to MG63 expression on 2D tissue culture polystyrene (TCPS) (set to 1-fold) for comparison.

2.10 Statistical analysis

All data was analyzed to express mean ± standard deviation unless stated otherwise. The data were analyzed using one-sided or two-sided analysis of variance (ANOVA) with post-hoc Tukey multiple comparisons testing for statistical significance ($p \leq 0.05$) in GraphPad Prism 7 (Prism version 7.04, Graph Pad Software, San Diego, CA).

3 Results and discussion

3.1 Base scaffold microstructure and other material properties

Repair of osteochondral defects requires simultaneous support of two cell populations, chondrogenic and osteogenic cells, that reside within distinct microenvironments – articular

cartilage and subchondral bone. Differing biochemical and biomechanical cues in each region makes scaffold design challenging, necessitating a multiphasic scaffold approach. To accurately mimic the layered osteochondral ECM, biochemical and biomechanical optimization of the cartilage and bone regions of a bilayer scaffold was necessary. Pure chitosan (C), chitosan-alginate (CA), and chitosan-hyaluronic acid (CHA) base scaffolds were each fabricated with two polymer concentrations (4 wt% and 6 wt%) per scaffold composition and screened as candidate scaffolds for the cartilage or bone layers of the target osteochondral bilayer scaffold. The polymer concentrations were selected based on previous studies showing 4 wt% CA scaffolds support osteogenic and chondrogenic cell culture (Li et al. 2005; Li and Zhang 2005). Scaffold pore structure and morphology, observed with SEM (Fig. 2a), displayed a defined, yet interconnected, open pore network for all scaffolds. Despite a similar overall polymer content, the 6% CA scaffolds had a significantly smaller mean pore cross-sectional area ($1.10 \pm 0.64 \times 10^4$ μm^2) than the 6% C scaffolds ($2.93 \pm 1.63 \times 10^4$ μm^2) likely due to the increased viscosity of the CA PEC ($p \leq 0.05$) (Fig. S1a). Scaffold density (Fig. 2b), which increased with polymer content, was different among all scaffold compositions, ranging from 0.04 g/cm^3 to 0.08 g/cm^3, and similar to values cited for other highly porous polymeric foams (Dorati et al. 2014).

Polymer content and density correlated with the compressive modulus or stiffness of the bulk, porous scaffold. The compressive modulus of dry and hydrated scaffolds increased as scaffold density increased (Fig. 2c, d). Overall, the CA scaffolds were the stiffest followed by the C scaffolds, and CHA scaffolds. The low compressive modulus of both dry and hydrated CHA scaffolds was due to low total polymer content relative to the other scaffold types.
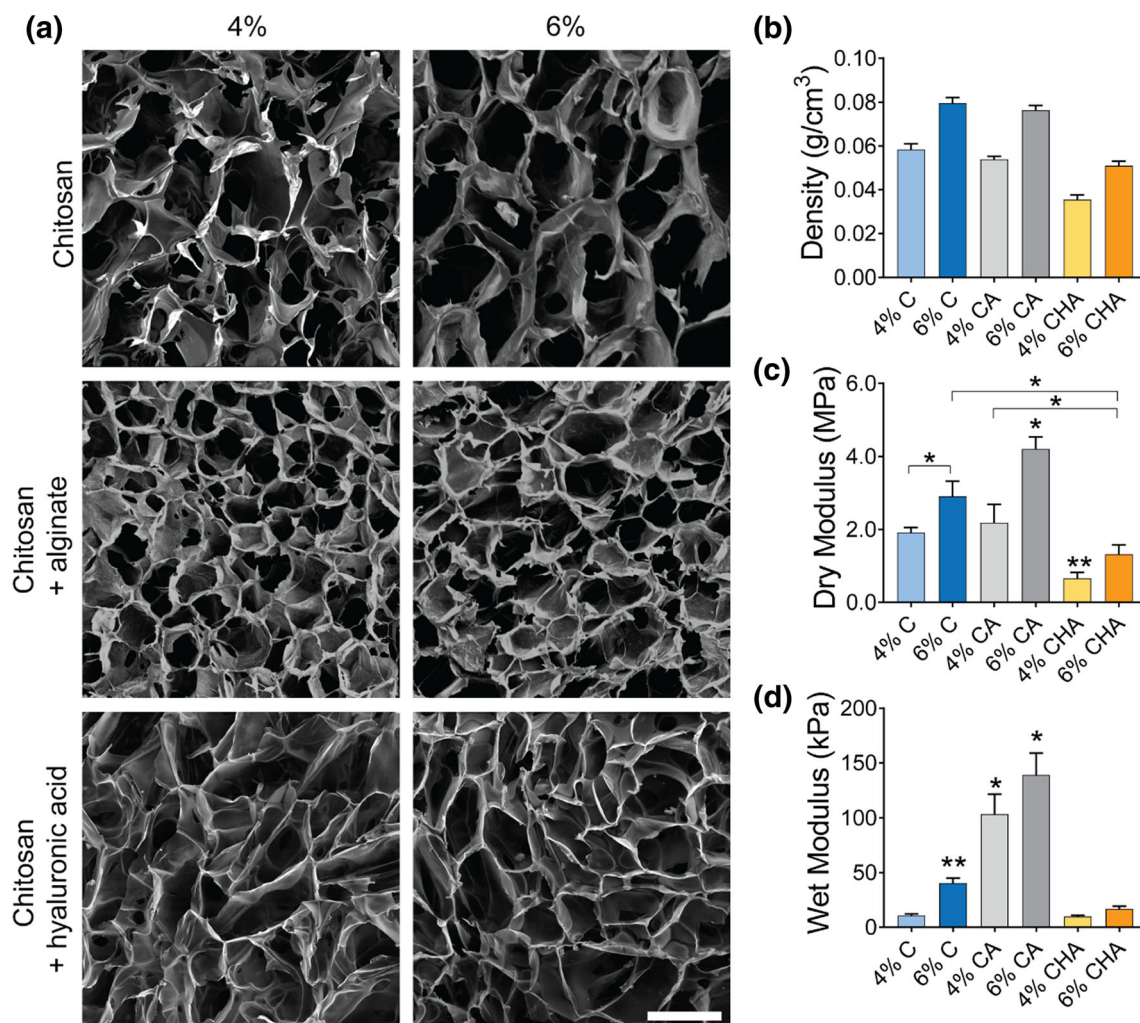

Fig. 2 Base scaffold microstructure and physical property characterization. **a** SEM images showing pore morphology. Scale bar is 200 μm. **b** Dry bulk density of all scaffolds significantly different ($p \leq 0.05$, $n = 12$). Compressive modulus of (**c**) dry scaffolds in MPa ($n = 4$) and (**d**) hydrated scaffolds in kPa ($n = 4$). *Statistically significant from all or specified conditions ($p \leq 0.05$). **Statistically significant from all conditions, except 6% CHA. ($p \leq 0.05$)

3.2 Cell attachment and proliferation on base scaffolds

In addition to characterizing and optimizing the physical properties of the scaffold to reflect the *in vivo* microenvironment, the response of relevant cells to the scaffold in terms of attachment and proliferation is also critical. Growth profiles for chondrocyte-like cells (SW-1353), rat bone marrow mesenchymal stem cells (MSC), and osteoblast-like cells (MG63) were established for each base scaffold by using the metabolic assay alamarBlue® (Fig. 3). The 4% CHA and 6% CHA scaffolds were seeded with chondrocyte-like SW-1353 or MSCs to evaluate their support of chondrogenic cells. Human SW-1353 cells have been utilized previously to evaluate cartilage regeneration (Cecen et al. 2016; Chien et al. 2012; Lu et al. 2015) and MSCs possess chondrogenic potential. The 4% and 6% C and CA scaffolds were seeded with osteoblast-like MG63, a cell line frequently used to evaluate osteogenic cell behavior on scaffolds (Gupta et al. 2016; Trombetta et al. 2017).

3.2.1 Cartilage layer scaffold

CHA scaffolds were evaluated as a potential chondral layer with the goal of mimicking native cartilage ECM compromised heavily of Glycosaminoglycans (GAGs). The structure of chitosan is similar to GAGs (Kim et al. 2008) and HA, a component of native articular cartilage, is important in tissue homeostasis and chondrogenesis (Kim et al. 2003; Knudson and Knudson 2004; Yoo et al. 2005). Combining chitosan and HA results in a stable PEC, blending the beneficial properties of both natural polymers. Lower polymer concentration scaffolds relative to bone layer scaffolds, as summarized in

Table 1, were investigated for the cartilage layer because chondrocytes prefer lower stiffness substrates relative to osteogenic cells. Additionally, lower stiffness substrates may influence mesenchymal stem cell fate toward a chondrogenic phenotype (Olivares-Navarrete et al. 2017).

In native articular cartilage, chondrocytes populate and deposit ECM to maintain healthy tissue. Cartilage layer bioactivity was evaluated using chondrocyte-like SW-1353 and MSCs with chondrogenic potential. An increase in metabolic activity from day 2 to day 10 was observed for SW-1353 and MSC cells in both 4% and 6% CHA scaffolds (Fig. 3a, b). The number of MSC cells on 4% CHA scaffolds was significantly higher than the number of MSCs on 6% CHA scaffolds at day 10. Based on proliferation and metabolic activity of the SW-1353 and MSC cells, 4% CHA scaffolds were selected for the cartilage layer of the osteochondral scaffold.

3.2.2 Bone layer scaffold

Subchondral bone, composed of type I collagen and calcium phosphate, is a stiffer tissue than cartilage. Presentation of appropriate stiffness cues is crucial to regeneration of healthy tissue because mechanosensing by stem cells is a key factor in lineage mediation. Determining the optimal bone layer base scaffold required a two-phase evaluation: (1) characterization of cell proliferation on higher stiffness scaffolds to identify the base scaffold material, and (2) addition of hydroxyapatite nanorods (HAp) and optimization of HAp content in the base scaffold to enhance scaffold osteoconductivity. Osteoblast-like MG63 cells were cultured on the four stiffest scaffolds (4% C, 6% C, 4% CA, and 6% CA summarized in Table 1) (Fig. 2c, d) resulting in increased metabolic activity for all scaffolds over the 10-day culture
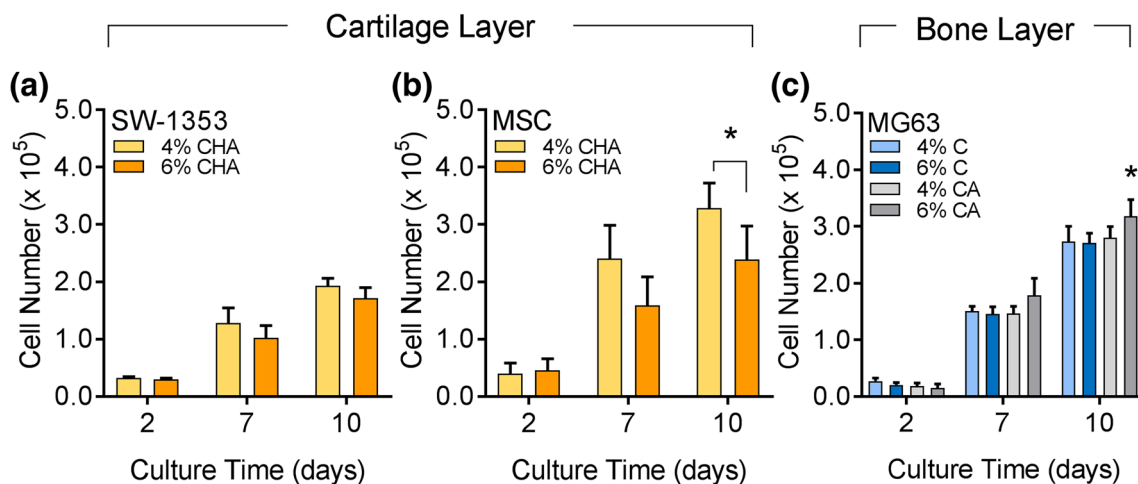

Fig. 3 Cell proliferation on base scaffolds. **a** SW-1353 and (**b**) MSC cultured on 4% and 6% CHA, and (**c**) MG63 cultured on 4% C, 6% C, 4% CA, and 6% CA for 10 days (n = 4). *Statistical significance within specified time point. (p ≤ 0.05)

period (Fig. 3c). At day 10, the number of MG63 cells on 6% CA scaffolds was significantly higher than on the C scaffolds or 4% CA scaffolds. The 6% CA scaffold was selected as the base material for the bone layer because of increased scaffold stiffness and superior support of osteogenic cell proliferation.

The addition of HAp, similar in composition to the inorganic component of bone (Batchelar et al. 2006; Malmberg and Nygren 2008), promotes osteogenesis when integrated into chitosan scaffolds (Chesnutt et al. 2009), and has shown promising results in bone TE *in vitro* and *in vivo*. Additionally, the scaffold with embedded nanorods mimics the native composite bone structure where mineralized calcium phosphate platelets and rods are embedded in a collagen matrix (Weiner and Wagner 1998). Therefore, to further enhance the bioactivity of the bone layer, hydroxyapatite nanorods were added to the 6% CA base scaffold (Fig. 4a, b). HAp nanorods were added in concentrations ranging from 0.1 wt% to 3 wt%. Pore morphologies in the HAp-integrated scaffolds was visualized with SEM (Fig. 4c**)**. All HAp-incorporated scaffolds possessed an open, porous structure indicating that HAp addition does not hinder pore formation during TIPS. As the HAp concentration within the CA scaffold increased up to 3%, the dry bulk density of the scaffolds also increased (Fig. 4d). Homogeneous HAp dispersal throughout the CA matrix was observed for all conditions, despite dispersal challenges cited in previous works (Venkatesan and Kim 2010). In the CA scaffold, the strong ionic interaction between alginate and Ca^{+2} in HAp acted as a dispersant (Kim et al. 2015).

The proliferative capacity of MG63 cells in HAp-integrated scaffolds was determined by evaluating metabolic activity (Fig. 4e). At day 7, no significant difference in metabolic activity was observed for cells cultured on CA scaffolds with or without HAp. By day 14, scaffolds with ≥1 wt% HAp began to disintegrate and release cells into suspension, resulting in decreased cell number. After two-weeks of culture, the 6% CA + 0.5% HAp scaffolds demonstrated aqueous stability while supporting proliferation of osteogenic cells. Therefore, this scaffold was selected for the osteochondral scaffold bone layer.

3.3 Bilayer scaffold architecture and mechanical properties

TE scaffolds must be biochemically suited for attachment and proliferation of the desired cell type. Nevertheless, appropriate scaffold structural cues are also essential to the generation of functional tissue. After evaluating six different scaffolds for supporting attachment and proliferation of the appropriate cell type, we found that SW-1353 and MSC cells prefer a higher HA content scaffold with

lower elastic modulus. The MG63 cells favor scaffolds with a higher elastic modulus and the highest HAp content while maintaining scaffold aqueous stability. By layering two polymer solutions with differing compositions and polymer contents (4% CHA and 6% CA + 0.5% HAp) before a single TIPS-lyophilization process, a gradient interface was achieved.

The resultant bilayer scaffold pore structure, including the interface region, was visualized via SEM (Fig. 5a–d). The interface between the two distinct layers of the scaffold was amalgamated and seamless (Fig. 5c) and the cartilage region (4% CHA) was less dense than the bone region (6% CA + HAp) (Fig. 5e). Scaffold porosity followed a similar trend, where the 4% CHA layer porosity was higher than the 6% CA + HAp layer porosity. Importantly, both regions were highly porous with >87% porosity. High porosity encourages recruitment and infiltration of native cells where the bioactive cues in each scaffold layer (i.e., HA and HAp) can help direct layer-specific ECM and tissue development. Pore size is a critical factor in cell attachment and infiltration, and can play a deterministic role in cell behavior (Di Luca et al. 2016). Due to the higher polymer content of the bone layer, 6% CA + HAp scaffold, the mean pore area was significantly smaller $(1.16 \pm 0.87 \times 10^4 \ \mu m^2)$ than the cartilage layer 4% CHA scaffold $(2.36 \pm 1.99 \times 10^4 \ \mu m^2)$ (Fig. S1b). Based on mean pore area and the assumption of circular pores to estimate mean pore diameter, the pore diameters would be approximately 145 μm (cartilage) and 110 μm (bone), respectively. These diameters fall in the range of relevant pore sizes for cell growth and tissue regeneration (Yang et al. 2001).

Pore size, shape, and interconnectivity in TIPS-fabricated scaffolds is dependent on the solution properties and processing temperatures. Development of a homogenous, isotropic pore structure requires uniform thermal energy transfer during freezing and lyophilizing. Layering different polymer solutions can result in non-uniform pore structures as the overlying solution has no direct contact with the freezing surface. Uniform conduction between the two polymer solutions is particularly important to ensure a consistent and integrated interface to mimic the calcified cartilage region, which should help prevent bone ingrowth in the cartilage region (Hunziker and Driesang 2003). Despite differing polymer solution densities and compositions, the freezing procedure reported here enabled ice crystal formation throughout the scaffold, as demonstrated by the consistent pore formation throughout the entirety of the bilayer scaffold. Further, pores bridge both scaffold layers, thereby creating a stable interface. A stable and interconnected interface is critical to prevent delamination, anchor the cartilage to the bone, and prevent zonal segregation from inhibiting integrated regeneration at the calcified cartilage interface (Kreklau et al. 1999; Niederauer et al. 2000).
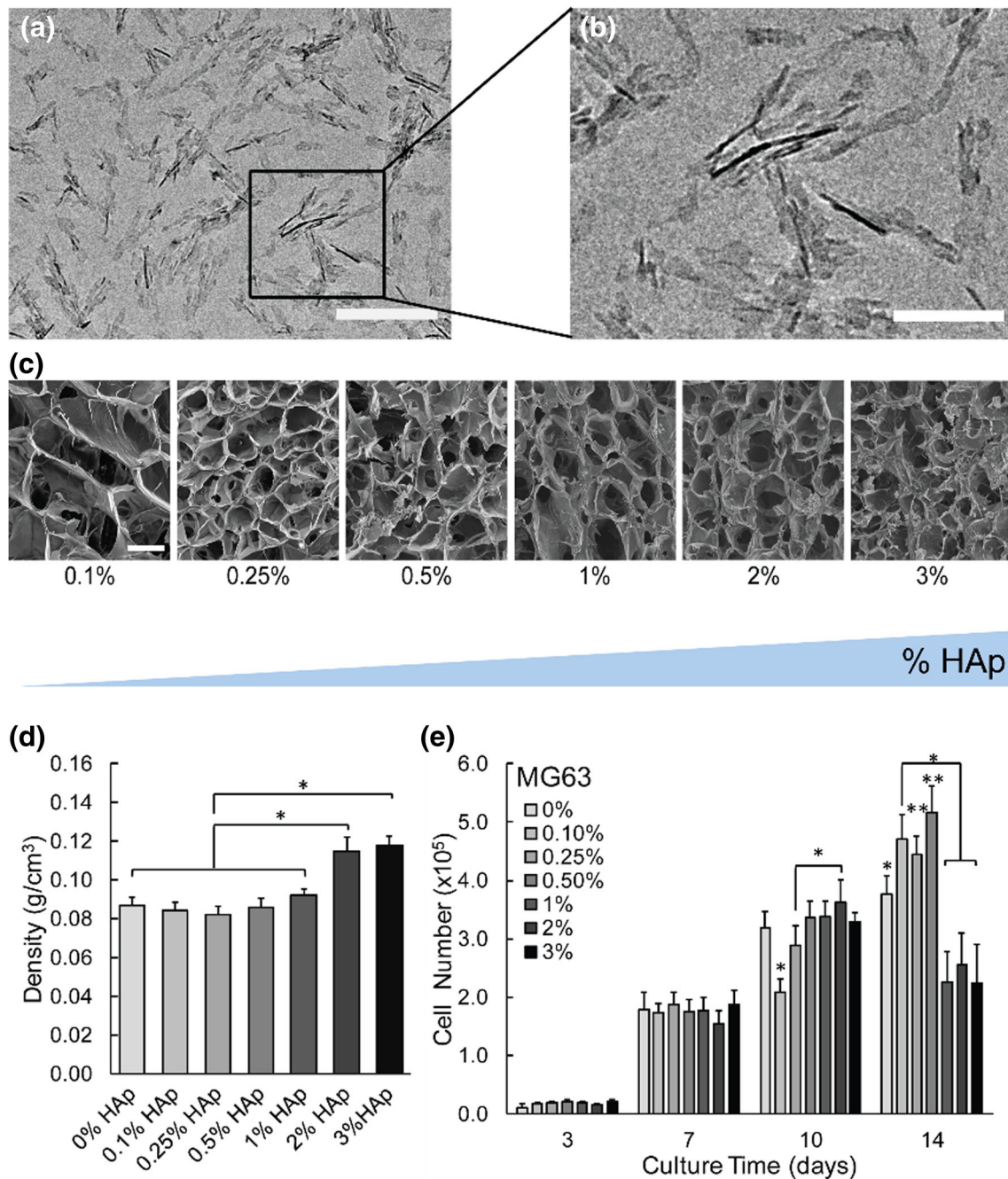
Fig. 4 Effect of HAp concentration on 6% CA scaffold properties. **a**, **b** Visualization of HAp nanorods with TEM. Scale bars represent 200 nm, and 100 nm, respectively, in (**a**) and (**b**). **c** SEM images of scaffold pore morphology with varying HAp (HAp concentration increases from left to right). Scale bar represents 200 μm. **d** Density of CA + HAp composite scaffolds ($n = 8$) (p ≤ 0.05). (**e**) MG63 proliferation on CA + HAp composite scaffolds over a 2-week culture period ($n = 4$). *Statistically significant from all or specified conditions (p ≤ 0.05). **Statistically significant from all conditions except 0.1% HAp (p ≤ 0.05)

The stiffness gradient between the cartilage and bone layers of a multiphasic, osteochondral TE scaffold is hypothesized to help mediate lineage in undifferentiated cells (Discher et al. 2005; Engler et al. 2006). This bilayer scaffold displayed stress-strain behavior typical for porous polymers (Frydrych et al. 2011) (Fig. 5g). Two distinct linear-elastic regions corresponding to each scaffold layer (Fig. 5h) suggest compression of the low stiffness region

(4% CHA) prior to the stiffer region (6% CA + HAp). Modulus 1 is defined by a compressive modulus of 6.90 ± 1.29 kPa, whereby Modulus 2 represents a stiffer region with a compressive modulus of 55.84 ± 16.0 kPa (Fig. 5h). Modulus 1 correlates with the modulus of a standalone 4% CHA scaffold (6.81 ± 0.70 kPa). The compressive modulus of a 6% CA + HAp scaffold was 139.0 ± 10.4 kPa, which is a 150% greater than Modulus 2,
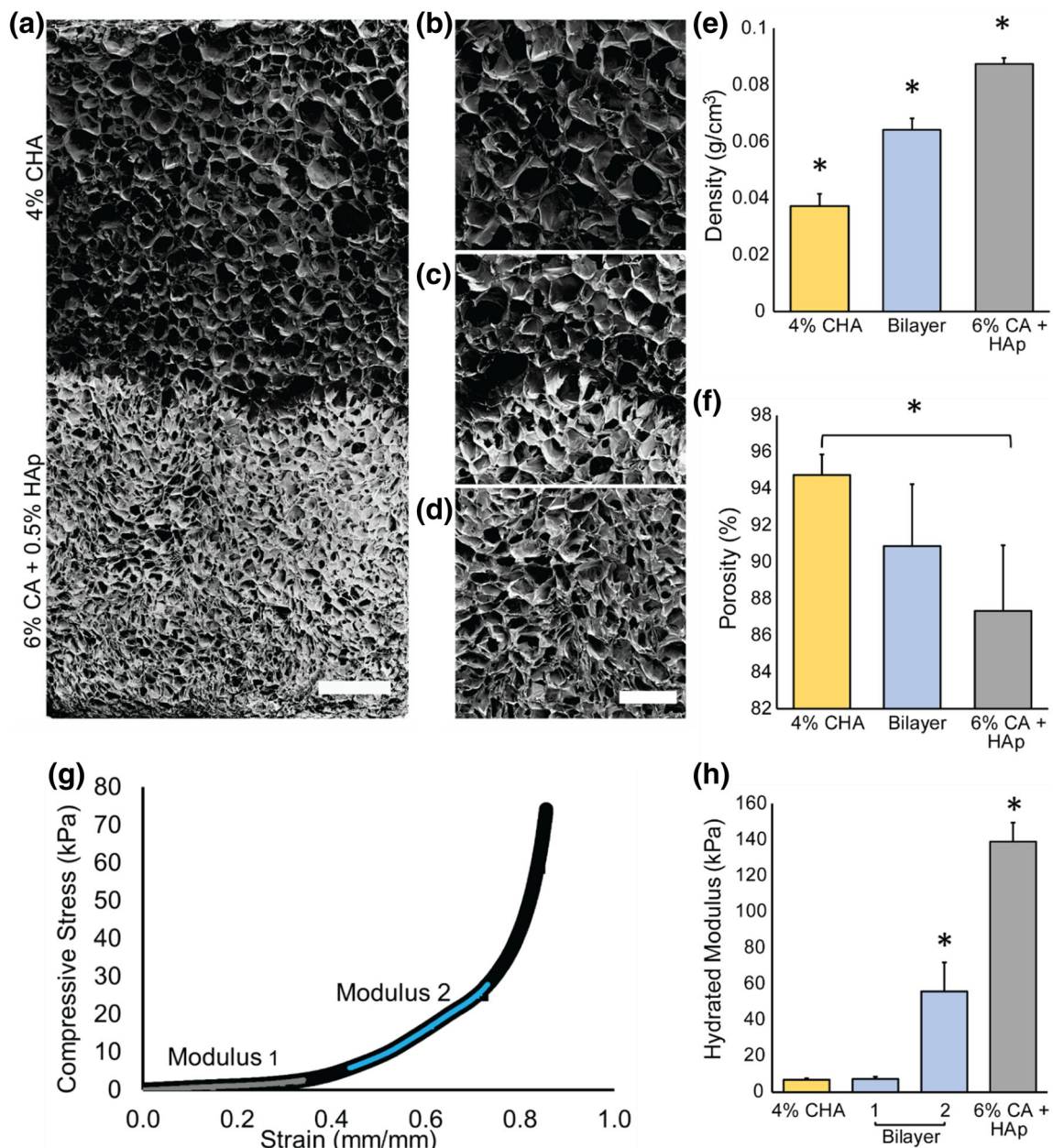
Fig. 5 Bilayer scaffold characterization. **a** SEM of bilayer scaffold with increased magnification of the (**b**) 4% CHA, (**c**) interface, and (**d**) 6% CA + 0.5% HAp layers. Scale bar represents 1 mm in (**a**) and 500 μm in (b-d). **e** Scaffold dry bulk density ($n = 4$). **f** Scaffold porosity (n = 4). **g** Representative compressive stress-strain curve for hydrated bilayer scaffold with modulus 1 corresponding to CHA region and modulus 2 corresponding to the CA + HAp region. **h** Compressive modulus of hydrated bilayer scaffold compared to pure components (n = 4). *Statistically significant from all or specified conditions ($p \leq 0.05$)

suggesting that modulus 2 in the bilayer scaffold had some contribution from both the cartilage (4% CHA) and bone (6% CA + HAp) layers indicating a stiffness gradient. In the native osteochondral microenvironment, the mechanical properties of the osteochondral region vary with patient age, activity, and location in the body, yet the compressive modulus has been cited at 98–270 MPa for subchondral bone (Schlichting et al. 2008) and 2–20 MPa for cartilage (Shepherd and Seedhom 1999). Despite advancements in materials and synthesis techniques, native osteochondral tissue has not been fully recapitulated using porous scaffolds. Polymeric scaffold stiffness is significantly less than native bone tissue, yet for non-load bearing bone or unique gradient microenvironments like the osteochondral tissue, a polymeric scaffold may be advantageous to promote healing at the interface. The stiffness of this bilayer scaffold is comparable to other natural polymer-based multiphasic scaffolds that have shown promise *in vivo* (Levingstone et al. 2014; Levingstone et al. 2016).

3.4 In vitro assessment of bilayer scaffold

Cell attachment, proliferation, and invasion in the bilayer scaffold was determined using two growth factor-free co-culture conditions over a two-week culture period. Scaffold co-cultures included: (1) SW-1353 + MG63 and (2) MSC + MG63. SW-1353 or MSC cells were seeded in the cartilage layer (4% CHA) and MG63 was seeded in the bone layer (6% CA + 0.5% HAp) to mimic native tissue (seeding illustrated in Fig. 1b). A significant increase in metabolic activity over a two-week culture period indicated the bilayer scaffold was amenable to simultaneous proliferation of these two co-cultures conditions (Fig. 6). Direct quantification of the specific contributions of each cell type to the increased metabolic activity or specific cell numbers associated with each cell line could not be determined using this assay model.

Cell migration and proliferation in each scaffold layer was visualized using fluorescence microscopy (Fig. 7). In the SW-1353 + MG63 co-culture condition (Fig. 7a, b), an increase in the number of SW-1353 (top, red) and MG63 (bottom, green) cells was observed near the seeding surfaces of the scaffold relative to the scaffold interior at day 1. By day 14, cell density increased in all scaffold layers, and cells appeared to invade the scaffold interior relative to day 1. SW-1353 cells were mostly present as single cells and small cell clusters whereas the MG63 cells formed larger cell clusters. Although sparse, both green and red cells were observed at the interface at day 1. By day 14, the interface displayed a higher density of both cell types, suggesting that both cell types penetrated the scaffold to the interface. At the interface, small cell clusters of SW-1353 and larger cell clusters of MG63 were observed.

An increase in cell number in both cartilage and bone regions was observed at day 14 in the bilayer scaffold co-

cultured with MSC + MG63 (Fig. 7c, d) as compared to the condition in the bilayer scaffold cocultured with SW-1353 + MG63, although the cell morphologies were similar under both conditions. MG63 cells in the bone layer (bottom, green) formed larger cell clusters than MSCs in the cartilage layer (top, red). Both cell types were present at the interface of the bilayer scaffold. SEM was used to examine cell morphology (Fig. 8). In the cartilage layer (CHA) (Fig. 8a, c), both SW-1353 and MSC cells in two different bilayer scaffolds assumed a rounded or spherical morphology. SW-1353 cells formed cell clusters, whereas MSC cells are present both in single cell state and in clusters. In the bone layer (CA + HAp) (Fig. 8b, d), MG63 cells showed their characteristic, spindle-like or elongated morphology, and spread along the pore walls. The MG63 cells formed large cell clusters as shown in the fluorescence images. In addition, it appears that a layer of extracellular fibrous matrix material was deposited on the highly populated cell areas of the scaffold making it difficult to identify the cell morphology.

To try to correlate increased proliferation with increased functionality, early chondrogenic (collagen type II) and osteogenic (osteocalcin) markers were evaluated using qRT-PCR. Type II collagen plays a critical role in stem cell and chondrocyte maturation and is vital to the development and formation of the GAG-rich articular cartilage (Bobick et al. 2009). For bone remodeling, osteocalcin is a known osteogenic marker (Marom et al. 2005) where increased expression signifies osteoblast maturation (Fig. 9). Each cell type was cultured separately on TCPS for comparison of gene expression in co-cultures on the bilayer scaffold relative to 2D TCPS. Gene expression for each condition was normalized to expression of the reference gene GAPDH. For comparison among 2D and co-culture conditions, gene expression was normalized to the 2D TCPS culture of MG63 (set to 1-

Fig. 6 Proliferation of chondrogenic and osteogenic cells in bilayer scaffold evaluated by measuring metabolic activity. Evaluation of (**a**) SW-1353 + MG63 and (**b**) MSC + MG63 metabolic activity measured with alamarBlue® ($n = 4$) *Statistical significance relative to all other time points. ($p \leq 0.05$)

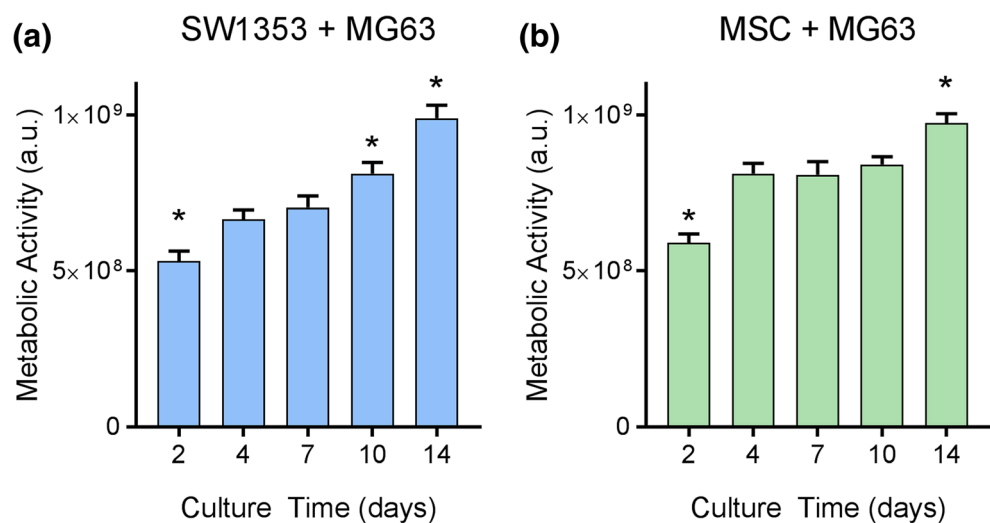**Fig. 7** Proliferation and migration of chondrogenic and osteogenic cells in bilayer scaffold cross-sections. Evaluation of SW-1353 + MG63 with (**a**) illustration of seeding condition and (**b**) fluorescence imaging of SW-1353 (red) and MG63 (green) in cartilage layer (top), interface (middle, marked by white triangles), and bone layer (bottom) of bilayer scaffold (blue auto fluorescence). Evaluation of MSC + MG63 with (**c**) illustration of seeding condition and (**d**) fluorescence imaging of MSC (red) and MG63 (green) in cartilage layer (top), interface (middle, marked by white triangles), and bone layer (bottom) of bilayer scaffold (blue auto fluorescence). Scale bar is 500 μm in (**b**) and (**d**)
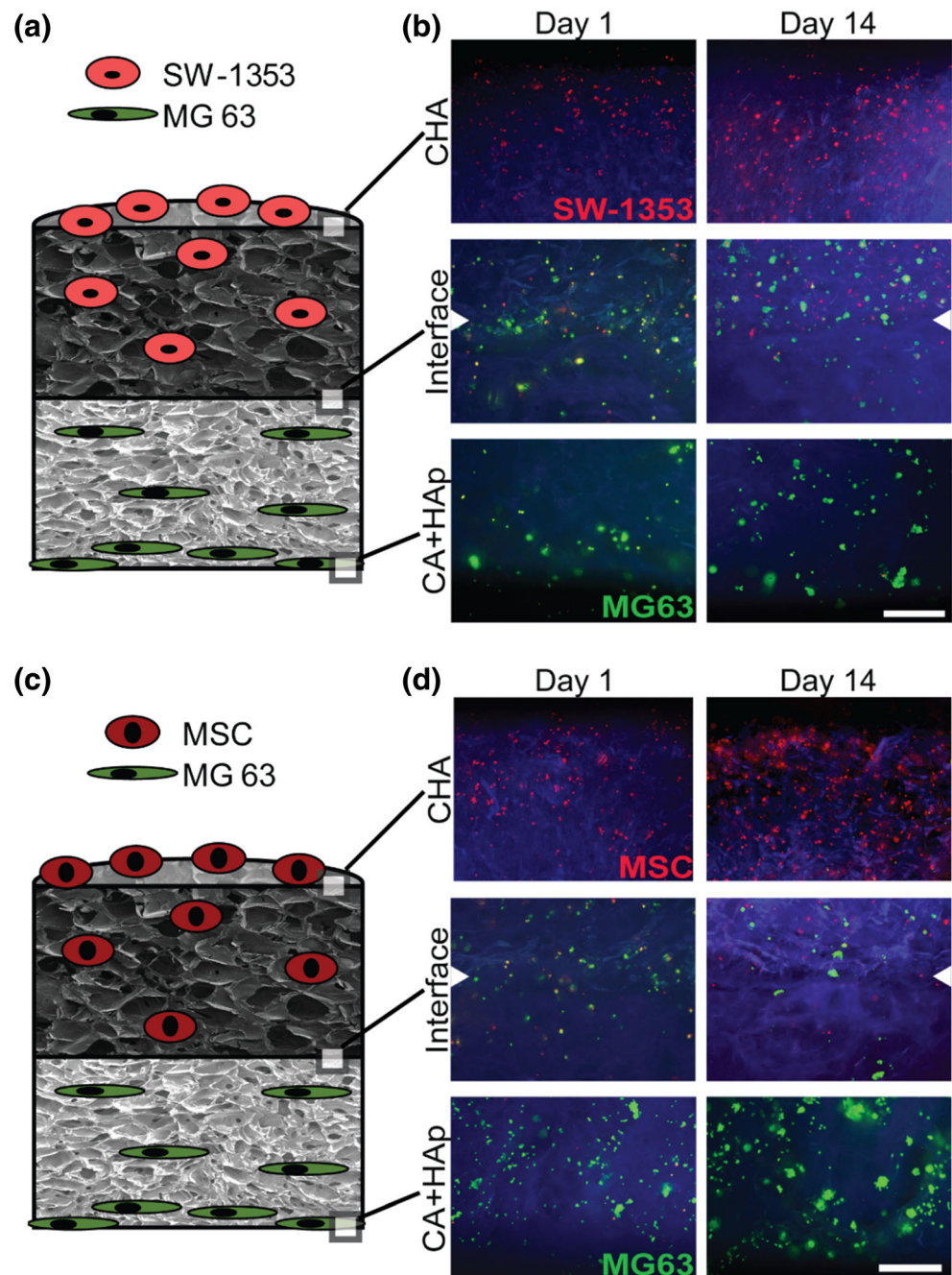
fold) because both co-cultures contained MG63 cells. Increased expression of chondrogenic and osteogenic markers was observed for both co-cultures on the bilayer scaffolds relative to all 2D cultures indicating that at early timepoints, chitosan-based bilayer scaffolds effectively support relevant cells.

Multiphasic scaffolds have shown promise in regeneration of layered tissues, yet current multiphasic scaffold design is hindered by time-consuming, iterative fabrication techniques and insufficient amalgamation between layers. Here, we designed a biomimetic, bilayer scaffold using a straightforward, fast, and pH-neutral, single-stage fabrication approach. Our layered TIPS approach overcomes the onerous, iterative fabrication requirements of previous technologies while maintaining tunability of each layer. Tailoring bioactive factors and mechanical gradients in multiphasic scaffold layers is vital to support synchronized regeneration. In osteochondral TE, specialized integration and segregation of bioactive factors specific to the bone region or the cartilage region is crucial to enhance zonal organization of the regenerated osteochondral tissue. By exploiting TIPS and the enhanced aqueous stability of PECs, a highly porous, bilayer scaffold was fabricated entirely using natural polymers.
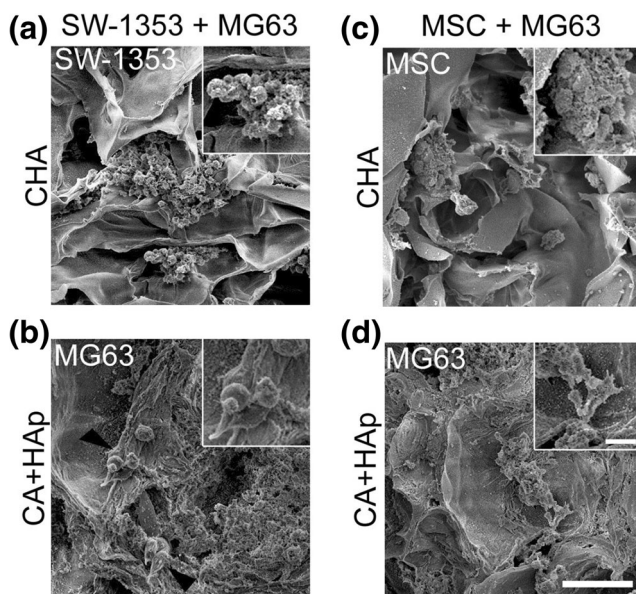
Fig. 8 SEM images of (**a, b**) SW1355 + MG63 and (**c, d**) MSC + MG63 **cells in** bilayer scaffolds after 2 weeks in culture. Scale bars represent 50 μm in images and 10 μm for insets

Natural polymers are advantageous over synthetic polymers because of their biocompatibility and biodegradability and chitosan, a major component of the bilayer scaffold, has previously been shown to support attachment and proliferation of both osteoblasts (Levengood and Zhang 2014; Li et al. 2005) and chondrocytes (Li and Zhang 2005). Importantly, the TIPS approach to layered scaffold fabrication has potential in osteochondral TE as well as for other complex layered tissues. By using a non-toxic, pH-neutral synthesis, future studies involving tailored growth factors integration could allow for sustained delivery and potential chemotactic recruitment of native cells directly to the defect site.
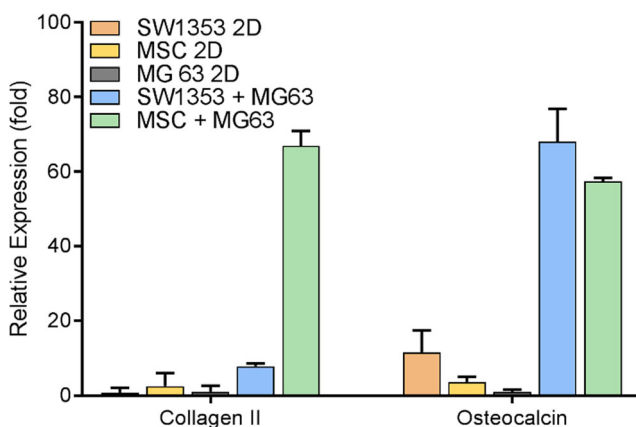

Fig. 9 Relative expression of RNA content in cells cultured on 2D TCPS (SW1353, MSC, and MG63) versus co-cultures in bilayer scaffolds (SW-1353 + MG63 and MSC + MG63). Gene expression was normalized to a reference gene, GAPDH, and then normalized to expression of MG63 on 2D TCPS (set as 1-fold). ($n = 3$)

4 Conclusion

We developed a bilayer, polysaccharide and GAG-based scaffold for osteochondral tissue regeneration using a simple, fast, and pH-neutral synthesis process. Each region of the bilayer scaffold was optimized with biomechanical and bioactive cues to enhance the proliferation of intended cell types (chondrogenic or osteogenic cells). Fabrication of this layered scaffold is advantageous over previously reported techniques due to the tunability of the elastic moduli of each layer as well as the integration of bioactive factors segregated to each specific region (HA in the cartilage region and HAp in the bone region). Additionally, the seamless gradient zone at the interface ensures stability by inhibiting delamination. The potential of this bilayer scaffold for osteochondral tissue engineering applications was characterized during a two-week co-culture where cell proliferation and infiltration to the scaffold interface was demonstrated.

References

H.M. Aydin, A three-layered osteochondral plug: Structural, mechanical, and in vitro biocompatibility analysis. Adv. Eng. Mater. **13**(12), B511–B517 (2011)

D.L. Batchelar, M.T.M. Davidson, W. Dabrowski, I.A. Cunningham, Bone-composition imaging using coherent-scatter computed tomography: Assessing bone health beyond bone mineral density. Med. Phys. **33**(4), 904–915 (2006)

J.E. Bekkers, T.S. de Windt, M. Brittberg, D.B. Saris, Cartilage repair in football (soccer) athletes: What evidence leads to which treatment? A critical review of the literature. Cartilage **3**(1 Suppl), 43S–49S (2012)

R. Bexkens, P.T. Ogink, J.N. Doornberg, G. Kerkhoffs, D. Eygendaal, L.S. Oh, M.P.J. van den Bekerom, Donor-site morbidity after osteochondral autologous transplantation for osteochondritis dissecans of the capitellum: A systematic review and meta-analysis. Knee Surg. Sports Traumatol. Arthrosc. **25**(7), 2237–2246 (2017)

B.E. Bobick, F.H. Chen, A.M. Le, R.S. Tuan, Regulation of the Chondrogenic phenotype in culture. Birth Defects Res. C. Embryo Today **87**(4), 351–371 (2009)

B. Cecen, L.D. Kozaci, M. Yuksel, O. Ustun, B.U. Ergur, H. Havitcioglu, Biocompatibility and biomechanical characteristics of loofah based scaffolds combined with hydroxyapatite, cellulose, poly-l-lactic acid with chondrocyte-like cells. Mater. Sci. Eng. C **69**, 437–446 (2016)

B.M. Chesnutt, A.M. Viano, Y. Yuan, Y. Yang, T. Guda, M.R. Appleford, et al., Design and characterization of a novel chitosan/nanocrystalline calcium phosphate composite scaffold for bone regeneration. J. Biomed. Mater. Res. A **88**(2), 491–502 (2009)

C.-S. Chien, H.-O. Ho, Y.-C. Liang, P.-H. Ko, M.-T. Sheu, C.-H. Chen, Incorporation of exudates of human platelet-rich fibrin gel in biodegradable fibrin scaffolds for tissue engineering of cartilage. J. Biomed. Mater. Res. B Appl. Biomater. **100B**(4), 948–955 (2012)

B.J. Cole, C. Pascual-Garrido, R.C. Grumet, Surgical management of articular cartilage defects in the knee. J. Bone Joint Surg. Am. **91**(7), 1778–1790 (2009)

A. Di Luca, B. Ostrowska, I. Lorenzo-Moldero, A. Lepedda, W. Swieszkowski, C. Van Blitterswijk, L. Moroni, Gradients in pore size enhance the osteogenic differentiation of human mesenchymal stromal cells in three-dimensional scaffolds. Sci. Rep. **6**, 22898 (2016)

D.E. Discher, P. Janmey, Y.L. Wang, Tissue cells feel and respond to the stiffness of their substrate. Science **310**(5751), 1139–1143 (2005)

R. Dorati, C. Colonna, C. Tomasi, I. Genta, G. Bruni, B. Conti, Design of 3D scaffolds for tissue engineering testing a tough polylactide-based graft copolymer. Mater. Sci. Eng. C Mater Biol Appl. **34**, 130–139 (2014)

A.J. Engler, S. Sen, H.L. Sweeney, D.E. Discher, Matrix elasticity directs stem cell lineage specification. Cell **126**(4), 677–689 (2006)

S.J. Florczyk, D.J. Kim, D.L. Wood, M. Zhang, Influence of processing parameters on pore structure of 3D porous chitosan-alginate polyelectrolyte complex scaffolds. J. Biomed. Mater. Res. A **98**(4), 614–620 (2011)

S.J. Florczyk, M. Leung, S. Jana, Z.S. Li, N. Bhattarai, J.I. Huang, et al., Enhanced bone tissue formation by alginate gel-assisted cell seeding in porous ceramic scaffolds and sustained release of growth factor. J. Biomed. Mater. Res. A **100A**(12), 3408–3415 (2012)

S.J. Florczyk, K. Wang, S. Jana, D.L. Wood, S.K. Sytsma, J.G. Sham, et al., Porous chitosan-hyaluronic acid scaffolds as a mimic of glioblastoma microenvironment ECM. Biomaterials **34**(38), 10143–10150 (2013)

S.J. Florczyk, F.M. Kievit, K. Wang, A.E. Erickson, R.G. Ellenbogen, M.Q. Zhang, 3D porous chitosan-alginate scaffolds promote proliferation and enrichment of cancer stem-like cells. J. Mater. Chem. B **4**(38), 6326–6334 (2016)

M. Frydrych, C.Y. Wan, R. Stengler, K.U. O'Kelly, B.Q. Chen, Structure and mechanical properties of gelatin/sepiolite nanocomposite foams. J. Mater. Chem. **21**(25), 9103–9111 (2011)

A. Galperin, R.A. Oldinski, S.J. Florczyk, J.D. Bryers, M.Q. Zhang, B.D. Ratner, Integrated bi-layered scaffold for osteochondral tissue engineering. Adv. Healthc. Mater. **2**(6), 872–883 (2013)

P. Gupta, M. Adhikary, J.C. M, M. Kumar, N. Bhardwaj, B.B. Mandal, Biomimetic, Osteoconductive non-mulberry silk Fiber reinforced Tricomposite scaffolds for bone tissue engineering. ACS Appl. Mater. Interfaces **8**(45), 30797–30810 (2016)

A. He, L. Liu, X. Luo, Y. Liu, F. Liu, X. Wang, et al., Repair of osteochondral defects with in vitro engineered cartilage based on autologous bone marrow stromal cells in a swine model. Sci. Rep. **7**, 40489 (2017)

Y.Y. Hsu, J.D. Gresser, D.J. Trantolo, C.M. Lyons, P.R.J. Gangadharam, D.L. Wise, Effect of polymer foam morphology and density on kinetics of in vitro controlled release of isoniazid from compressed foam matrices. J. Biomed. Mater. Res. **35**(1), 107–116 (1997)

E.B. Hunziker, Articular cartilage repair: Basic science and clinical progress. A review of the current status and prospects. Osteoarthr. Cartil. **10**(6), 432–463 (2002)

E.B. Hunziker, I.M. Driesang, Functional barrier principle for growth-factor-based articular cartilage repair. Osteoarthr. Cartil. **11**(5), 320–327 (2003)

S. Jana, S.J. Florczyk, M. Leung, M.Q. Zhang, High-strength pristine porous chitosan scaffolds for tissue engineering. J. Mater. Chem. **22**(13), 6291–6299 (2012)

X. Jin, J. Zhuang, Z. Zhang, H. Guo, J. Tan, Hydrothermal synthesis of hydroxyapatite nanorods in the presence of sodium citrate and its aqueous colloidal stability evaluation in neutral pH. J. Colloid Interface Sci. **443**, 125–130 (2015)

F.M. Kievit, S.J. Florczyk, M.C. Leung, O. Veiseh, J.O. Park, M.L. Disis, M. Zhang, Chitosan-alginate 3D scaffolds as a mimic of the glioma tumor microenvironment. Biomaterials **31**(22), 5903–5910 (2010)

G. Kim, M. Okumura, T. Ishiguro, T. Kadosawa, T. Fujinaga, Preventive effect of hyaluronic acid on the suppression of attachment and migration abilities of bovine chondrocytes by IL-1 alpha in vitro. J. Vet. Med. Sci. **65**(3), 427–430 (2003)

I.Y. Kim, S.J. Seo, H.S. Moon, M.K. Yoo, I.Y. Park, B.C. Kim, C.S. Cho, Chitosan and its derivatives for tissue engineering applications. Biotechnol. Adv. **26**(1), 1–21 (2008)

H.L. Kim, G.Y. Jung, J.H. Yoon, J.S. Han, Y.J. Park, D.G. Kim, et al., Preparation and characterization of nano-sized hydroxyapatite/alginate/chitosan composite scaffolds for bone tissue engineering. Mater. Sci. Eng. C Mater. Biol. Appl. **54**, 20–25 (2015)

C.B. Knudson, W. Knudson, Hyaluronan and CD44: Modulators of chondrocyte metabolism. Clin. Orthop. Relat. Res. (427 Suppl), S152–S162 (2004)

E. Kon, M. Delcogliano, G. Filardo, M. Fini, G. Giavaresi, S. Francioli, et al., Orderly osteochondral regeneration in a sheep model using a novel nano-composite multilayered biomaterial. J. Orthop. Res. **28**(1), 116–124 (2010)

B. Kreklau, M. Sittinger, M.B. Mensing, C. Voigt, G. Berger, G.R. Burmester, et al., Tissue engineering of biphasic joint cartilage transplants. Biomaterials **20**(18), 1743–1749 (1999)

S.L. Levengood, M. Zhang, Chitosan-based scaffolds for bone tissue engineering. J. Mater. Chem. B **2**(21), 3161–3184 (2014)

T.J. Levingstone, A.C. Ramesh, R.T. Brady, P. Brama, J.P. Gleeson, F.J. O'Brien, Collagen-based multilayered scaffold shows potential for osteochondral defect repair. J. Tissue Eng. Regen. Med. **8**, 82–83 (2014)

T.J. Levingstone, E. Thompson, A. Matsiko, A. Schepens, J.P. Gleeson, F.J. O'Brien, Multi-layered collagen-based scaffolds for osteochondral defect repair in rabbits. Acta Biomater. **32**, 149–160 (2016)

Z.S. Li, M.Q. Zhang, Chitosan-alginate as scaffolding material for cartilage tissue engineering. J. Biomed. Mater. Res. A **75A**(2), 485–493 (2005)

Z.S. Li, H.R. Ramay, K.D. Hauch, D.M. Xiao, M.Q. Zhang, Chitosan-alginate hybrid scaffolds for bone tissue engineering. Biomaterials **26**(18), 3919–3928 (2005)

E. Lopez-Ruiz, G. Jimenez, M.A. Garcia, C. Antich, H. Boulaiz, J.A. Marchal, M. Peran, Polymers, scaffolds and bioactive molecules with therapeutic properties in osteochondral pathologies: what's new? Expert Opin. Ther. Pat. **26**(8), 877–890 (2016)

H.-T. Lu, M.-S. Hsieh, C.-W. Cheng, L.-F. Yao, T.-Y. Hsu, J. Lan, et al., Alterative effects of an oral alginate extract on experimental rabbit osteoarthritis. J. Biomed. Sci. **22**(1), 64 (2015)

H. Madry, C.N. van Dijk, M. Mueller-Gerbl, The basic science of the subchondral bone. Knee Surg. Sports Traumatol. Arthrosc. **18**(4), 419–433 (2010)

P. Malmberg, H. Nygren, Methods for the analysis of the composition of bone tissue, with a focus on imaging mass spectrometry (TOF-SIMS). Proteomics **8**(18), 3755–3762 (2008)

R. Marom, I. Shur, R. Solomon, D. Benayahu, Characterization of adhesion and differentiation markers of osteogenic marrow stromal cells. J. Cell. Physiol. **202**(1), 41–48 (2005)

T. Nie, L. Xue, M. Ge, H. Ma, J. Zhang, Fabrication of poly(L-lactic acid) tissue engineering scaffolds with precisely controlled gradient structure. Mater. Lett. **176**, 25–28 (2016)

G.G. Niederauer, M.A. Slivka, N.C. Leatherbury, D.L. Korvick, H.H. Harroff, W.C. Ehler, et al., Evaluation of multiphase implants for repair of focal osteochondral defects in goats. Biomaterials **21**(24), 2561–2574 (2000)

S.H. Oh, I.K. Park, J.M. Kim, J.H. Lee, In vitro and in vivo characteristics of PCL scaffolds with pore size gradient fabricated by a centrifugation method. Biomaterials **28**(9), 1664–1671 (2007)

S.H. Oh, T.H. Kim, J.H. Lee, Creating growth factor gradients in three dimensional porous matrix by centrifugation and surface immobilization. Biomaterials **32**(32), 8254–8260 (2011)

R. Olivares-Navarrete, E.M. Lee, K. Smith, S.L. Hyzy, M. Doroudi, J.K. Williams, et al., Substrate stiffness controls osteoblastic and Chondrocytic differentiation of mesenchymal stem cells without exogenous stimuli. PLoS One **12**(1), e0170312 (2017)

D. Schaefer, I. Martin, G. Jundt, J. Seidel, M. Heberer, A. Grodzinsky, et al., Tissue-engineered composites for the repair of large osteochondral defects. Arthritis Rheum. **46**(9), 2524–2534 (2002)

M. Schinhan, M. Gruber, P. Vavken, R. Dorotka, L. Samouh, C. Chiari, et al., Critical-size defect induces unicompartmental osteoarthritis in a stable ovine knee. J. Orthop. Res. **30**(2), 214–220 (2012)

K. Schlichting, H. Schell, R.U. Kleemann, A. Schill, A. Weiler, G.N. Duda, D.R. Epari, Influence of scaffold stiffness on subchondral bone and subsequent cartilage regeneration in an ovine model of osteochondral defect healing. Am. J. Sports Med. **36**(12), 2379–2391 (2008)

S.-J. Seo, C. Mahapatra, R.K. Singh, J.C. Knowles, H.-W. Kim, Strategies for osteochondral repair: Focus on scaffolds. J. Tissue Eng. **5**, 2041731414541850–2041731414541850 (2014)

D.E. Shepherd, B.B. Seedhom, The 'instantaneous' compressive modulus of human articular cartilage in joints of the lower limb. Rheumatology (Oxford) **38**(2), 124–132 (1999)

R. Shu, R. McMullen, M.J. Baumann, L.R. McCabe, Hydroxyapatite accelerates differentiation and suppresses growth of MC3T3-E1 osteoblasts. J. Biomed. Mater. Res. A **67A**(4), 1196–1204 (2003)

Y.P. Singh, J.C. Moses, B.K. Bhunia, S.K. Nandi, B.B. Mandal, Hierarchically structured seamless silk scaffolds for osteochondral interface tissue engineering. J. Mater. Chem. B **6**(36), 5671–5688 (2018)

G.D. Smith, G. Knutsen, J.B. Richardson, A clinical review of cartilage repair techniques. J. Bone Joint Surg. Br. Vol. **87B**(4), 445–449 (2005)

R. Trombetta, J.A. Inzana, E.M. Schwarz, S.L. Kates, H.A. Awad, 3D printing of calcium phosphate ceramics for bone tissue engineering and drug delivery. Ann. Biomed. Eng. **45**(1), 23–44 (2017)

J. Venkatesan, S.-K. Kim, Chitosan composites for bone tissue engineering—An overview. Mar. Drugs. **8**(8), 2252–2266 (2010)

K. Wang, F.M. Kievit, A.E. Erickson, J.R. Silber, R.G. Ellenbogen, M.Q. Zhang, Culture on 3D chitosan-hyaluronic acid scaffolds enhances stem cell marker expression and drug resistance in human glioblastoma Cancer stem cells. Adv. Healthc. Mater. **5**(24), 3173–3181 (2016)

S. Weiner, H.D. Wagner, THE MATERIAL BONE: Structure-mechanical function relations. Annu. Rev. Mater. Sci. **28**(1), 271–298 (1998)

S. Yang, K.F. Leong, Z. Du, C.K. Chua, The design of scaffolds for use in tissue engineering. Part I. Traditional factors. Tissue Eng. **7**(6), 679–689 (2001)

H.S. Yoo, E.A. Lee, J.J. Yoon, T.G. Park, Hyaluronic acid modified biodegradable scaffolds for cartilage tissue engineering. Biomaterials **26**(14), 1925–1933 (2005)

P. Yusong, S. Qianqian, P. Chengling, W. Jing, Prediction of mechanical properties of multilayer gradient hydroxyapatite reinforced poly(vinyl alcohol) gel biomaterial. J. Biomed. Mater. Res. B Appl. Biomater. **101B**(5), 729–735 (2013)

R.Y. Zhang, P.X. Ma, Poly(alpha-hydroxyl acids) hydroxyapatite porous composites for bone-tissue engineering. I. Preparation and morphology. J. Biomed. Mater. Res. **44**(4), 446–455 (1999)